THE ASTROPHYSICAL JOURNAL, 492:228–245, 1998 January 1

HARD X-RAYS AND GAMMA RAYS FROM TYPE Ia SUPERNOVAE

P. HÖFLICH,[1,2] J. C. WHEELER,[1] AND A. KHOKHLOV[3]
Received 1997 February 14; accepted 1997 August 6

ABSTRACT

The γ-ray light curves and spectra are presented for a set of theoretical Type Ia supernova (SN Ia) models including deflagration, detonation, delayed detonation, and pulsating delayed detonations of Chandrasekhar-mass white dwarfs, as well as merger scenarios that may involve more than the Chandrasekhar mass and helium detonations of sub–Chandrasekhar-mass white dwarfs. The results have been obtained with a Monte Carlo radiation transport scheme that takes into account all relevant γ-transitions and interaction processes. The result is a set of accurate line profiles that are characteristic of the initial ^{56}Ni mass distribution of the supernova models. The γ-rays probe the isotopic rather than merely the elemental distribution of the radioactive elements in the ejecta. Details of the line profiles (including the line width, shift with respect to the rest frame, and line ratios) are discussed. With sufficient energy and temporal resolution, different model scenarios can clearly be distinguished. Observational strategies are discussed for current and immediately upcoming generations of satellites (*Compton Gamma Ray Observatory* [*CGRO*] and *International Gamma-Ray Astrophysical Laboratory* [*INTEGRAL*]), as well as projected future missions including presently unavailable equipment such as Laue telescopes. With *CGRO*, it is currently possible with sufficiently early observations (near optical maximum) to distinguish helium detonations from explosions of Chandrasekhar-mass progenitors and of those involving mergers up to a distance of about 15 Mpc. This translates into one target of opportunity every 8 years. SNe Ia up to about 10 Mpc would allow detailed *CGRO* studies of line ratios of ^{56}Co lines. *INTEGRAL* will be able to perform detailed studies of the ^{56}Co line profiles with a range comparable to *CGRO*. The superior sensitivity of *INTEGRAL* for low energies makes detection and detailed study of the positron annihilation line and appropriate low-energy ^{56}Ni lines possible up to about 10–15 Mpc for all models. This capability means that this lower energy range may be the most useful for *INTEGRAL* detection and study of SNe Ia. Such studies will allow the determination of the precise time of the explosion. Whereas the current generation of γ-ray detectors will allow the study of supernovae that are discovered by other means, a new generation of proposed γ-ray detectors with sensitivity of about 10^{-6} photons s^{-1} cm^{-2} would generate the opportunity to discover supernovae by their γ-ray emission up to a distance of $\approx$100 Mpc. This would allow a systematic study of the variety of SNe Ia in terms of their γ-ray properties, independent of their optical properties. In addition, since γ-rays are not obscured by the host galaxy, such experiments would, for the first time, provide absolute supernova rates. Relative rates as a function of the morphology of and position in the host galaxy could be studied directly.

Subject headings: gamma rays: theory — nuclear reactions, nucleosynthesis, abundances — supernovae: general — supernova remnants

1. INTRODUCTION

Type Ia supernovae (SNe Ia) are among the most spectacular explosive events. They are major contributors to the production of heavy elements and hence a critical component for understanding the life cycles of matter in the universe and the chemical evolution of galaxies. While much progress has been made on understanding the underlying physics of the thermonuclear explosion (Khokhlov, Oran, & Wheeler 1997a, 1997b; Niemeyer & Woosley 1997), the basic processes require further elucidation and testing, and the progenitor evolution is still a deep mystery (Wheeler 1996). The great brightness of SNe Ia has made them a valuable tool for the measurement of extragalactic distances (Freedman et al. 1994) and for determining the shape of the universe (Perlmutter et al. 1995; Schmidt et al. 1997). The absolute brightness must be known either by using other distance calibrators (Hamuy et al. 1996; Riess, Press, & Kirshner 1996; Sandage & Tammann 1996) or theoretical models for the light curves and spectra (Höflich 1995; Höflich & Khokhlov 1996, hereafter HK96). A detailed physical understanding of SNe Ia is important for its own sake. In addition, such a physical understanding is necessary to constrain systematic errors when using them at high redshifts to determine the deceleration parameter q_0 and other cosmological parameters. Evolutionary effects on the progenitor population, such as the initial mass function (IMF) and metallicity, are expected to produce systematic errors (Höflich et al. 1997).

It is widely accepted that SNe Ia are thermonuclear explosions of carbon-oxygen white dwarfs; however, three groups of progenitor models can be distinguished. The first group consists of carbon-oxygen white dwarfs close to the Chandrasekhar mass that accrete mass through Roche lobe overflow from an unevolved (cataclysmic-variable–like) or evolved companion star. In these accretion models, the explosion is triggered by compressional heating. From the theoretical standpoint, the two key issues here are the conditions under which the thermonuclear explosion starts and

[1] Department of Astronomy, University of Texas, Austin, TX 07871.
[2] Department of Physics, University of Basel, CH-7046 Basel, Switzerland.
[3] Laboratory for Computational Physics and Fluid Dynamics, Code 6404, Naval Research Laboratory, Washington, DC 20375.

how the flame propagates through the white dwarf. The ignition and propagation may be affected by the rotation and mass accretion rate of the white dwarf, which will in turn be affected by the metallicity, age, and population of the progenitor system. The second group of progenitor models features two low-mass white dwarfs in a close orbit that decays as a result of the emission of gravitational radiation. This eventually leads to the merging of the two white dwarfs. In this scenario, the total mass of the merged object may exceed the Chandrasekhar mass and rotation may play an especially significant role. A third class of models are those involving helium detonations, i.e., double detonation of a C-O white dwarf triggered by the detonation of an outer helium layer in low-mass white dwarfs. Each of these scenarios has different implications for the resulting supernova statistics, the evolutionary ages of the progenitor systems, and the chemical evolution of galaxies and the universe.

Gamma rays are of particular interest as a diagnostic tool of these various progenitor models because they allow the direct observation of radioactive isotopes that power the observable light curves and spectra. Almost three decades ago Clayton, Colgate, & Fishman (1969) pointed out that the γ-ray lines from SN Ia explosions should be detectable at distances up to a few Mpc. Since then many authors have studied the γ-ray signatures of SNe Ia (Clayton 1974; Ambwani & Sutherland 1988; Chan & Lingenfelter 1988, 1990, 1991; Burrows & The 1990; Burrows et al. 1991; Höflich, Khokhlov, & Müller 1992, 1993a, 1993b, 1994; Kumagai & Nomoto 1997). These studies have shown that γ-ray observations of SNe Ia provide a powerful diagnostic tool to test proposed theoretical models. The key role of γ-rays for understanding of SNe Ia became obvious in the case of the peculiar SN 1991T. Because of the lack of γ-ray detection and/or firm upper limits, the nature of SN 1991T was not fully revealed despite various efforts (Höflich et al. 1994; Kumagai & Nomoto 1997) and an excellent set of data from the optical to the IR (e.g., Meikle et al. 1996) and even a distance from δ Cephei stars (Saha et al. 1996). Nevertheless, this event clearly showed the potential and implications for γ-ray observations (e.g., Lichti et al. 1994; Leising et al. 1995, and references therein).

Although systematic studies of the γ-ray emission properties of different scenarios have been published, several scenarios, some of them with rather strong observational and physical support, have not been considered (e.g., Burrows & The 1990; Chan & Lingenfelter 1990, 1991; Höflich et al. 1992), or where both Chandrasekhar-type and sub-Chandrasekhar–type models have been included, no detailed study of line profiles has been performed (e.g., Kumagai & Nomoto 1997).

In addition, little attention has been paid to specific observational strategies and the information required to allow instrument designers to estimate the performance of their instruments and to analyze future data. A detailed knowledge of the line position is critical for instruments that provide only a very limited wavelength range, such as the Laue telescopes currently in the design phase. Even for conventional γ-ray telescopes such as the *Compton Gamma Ray Observatory* (*CGRO*) or the upcoming *International Gamma-Ray Astrophysical Laboratory* (*INTEGRAL*), the detection limits may improve if information on the line position and profile is taken into account. Because of the low signal-to-noise ratio, detectibility is greatly dependent on the line profile and on the knowledge of the line position. In principle, the information from the models and the measurement can be combined during the data analysis to filter out the high noise, rather than comparing predicted and observed fluxes after the reductions.

This paper will seek to fill some of the gaps just mentioned. In the next section we describe briefly the numerical methods and the hydrodynamical models on which this study is based. In § 3, the properties of line profiles are quantitatively discussed along with the γ-ray light curves. In § 4, the expected rate and the possible applications for supernova searches with current and future instruments are briefly discussed. Section 5 presents a final discussion and conclusions.

2. BRIEF DESCRIPTION OF THE NUMERICAL METHODS

2.1. *Hydrodynamics*

The dynamical explosion models are calculated using a one-dimensional Lagrangian hydrocode with an artificial viscosity (Khokhlov 1991) and a radiation hydrodynamic code that includes nuclear networks (HK96 and references therein). The latter code is based on the light-curve code presented in (Höflich et al. 1993a) that solves the hydrodynamic equations explicitly by the piecewise parabolic method (Collela & Woodward 1984). This code includes the solution of the radiation transport implicitly via the moment equations, expansion opacities, and a detailed equation of state. Typically, 300 to 500 depth points are used. The γ-ray transport is omitted during the hydrodynamic phase because of the high optical depth of the inner layers. Nuclear burning is taken into account using Thielemann's network (Thielemann, Nomoto, & Hashimoto 1994 and references therein). During the hydrodynamic phase, an α-network of 20 isotopes is considered to properly describe the energy release. The final chemical structure is calculated by postprocessing the hydrodynamic model using a network of 216 isotopes.

2.2. *Gamma-Ray Transport*

For a given explosion model, γ-rays are calculated using a detailed Monte Carlo γ-ray transport scheme (Höflich et al. 1992, 1993b). A Monte Carlo scheme has been used because of its flexibility with respect to the treatment of physical processes, because relativistic effects can be included in a straightfoward way, and because it allows for a consistent treatment of both the continua and lines.

Photons are initialized in the transport code according to the distribution of ^{56}Ni and ^{56}Co in the hydrodynamic model. All ^{56}Ni (six) and ^{56}Co (46) decay lines have been taken into account. For the β^+ decay, the assumption is made that all positrons form positronium at the point where they are produced by radioactive decay and hence that they decay locally to produce annihilation photons. The positron leakage can be neglected during the first few months, but it may become important during late stages, especially for low-mass envelopes or if the ^{56}Ni is located in the outer layers. (For a discussion of positron leakage, see Colgate, Fryer, & Hand 1997 and references therein.) About $(1–5) \times 10^6$ initial decay photons are created for each Monte Carlo calculation. The direction of the photons is chosen randomly in the comoving frame of the expanding matter. Following Ambwani & Sutherland (1988), we have included the following three interaction processes in the

Monte Carlo transport code: Compton scattering according to the full angle-dependent Klein-Nishina formula, pair-production with cross section taken from Hubbell (1969), and photoelectric absorption with cross sections determined on the basis of the tables given by Veigele (1973). The emergent γ-ray spectra have been calculated with a high energy resolution of $\lambda/\delta\lambda = 600$. This resolution is sufficient to obtain accurate line profiles and fluxes. For more details, see Höflich et al. (1992).

3. DYNAMICAL MODELS

The γ-ray spectra have been computed for a large variety of models including delayed detonations (the DD series of Höflich et al. 1997), pulsating delayed detonations (the PDD series presented in Khokhlov, Müller, & Höflich 1992, Höflich, Khokhlov, & Wheeler 1995, and HK96), binary white dwarf merger scenarios (the DET2env series of Khokhlov, Müller, & Höflich 1993), and helium detonation models (the HeD series of HK96). The classical detonation scenarios are omitted because this class of models is known to produce hardly any intermediate-mass elements and hence to fail by inspection the criterion of agreement with spectral observations.

The first group of models we consider (the delayed detonation and pulsating delayed detonation models) consists of carbon-oxygen white dwarfs with a mass close to the Chandrasekhar limit. These systems presumably result from accretion through Roche lobe overflow from a companion star (Nomoto & Sugimoto 1977; Nomoto 1982). In these accretion models, the explosion is triggered by compressional heating and the heat wave traveling inward from any nuclear shell burning region at the surface. Typically, the thermonuclear runaway occurs at central densities $\rho_c \approx (2\text{–}3) \times 10^9$ g cm^{-3}. In the innermost regions, burning occurs at low Y_e, and consequently, neutron-rich isotopes are produced rather than ^{56}Ni, as shown in Figure 1 (*top left*).

The second group of progenitor models is based on the scenario of two low-mass white dwarfs in a close orbit that decays as a result of the emission of gravitational radiation, thus leading eventually to the merging of the two white dwarfs as the smaller mass, larger radius white dwarf fills its Roche lobe first and undergoes unstable mass transfer (Iben & Tutukov 1984; Webbink 1984). The combined mass of the two white dwarfs exceeds the Chandrasekhar limit, but the larger mass white dwarf that receives the mass is nevertheless itself below the Chandrasekhar limit. Its subsequent carbon ignition is expected to occur at low density as mass accretes from the extended C-O envelope formed by the disrupted star (Benz et al. 1990). Since burning occurs at low densities, there is little neutronization and ^{56}Ni is produced in the center (Fig. 1, *top right*).

The third class of models explored here is based on low-mass white dwarfs in which a degenerate helium layer builds up on top of a degenerate C-O core. The explosion is triggered by detonation of the helium layer, which then (in some circumstances) causes the inner C-O core to detonate as well. This scenario for normally bright SNe Ia was explored by Nomoto (1981), Woosley, Weaver, & Taam (1980), and most recently by Livne & Glasner (1990),

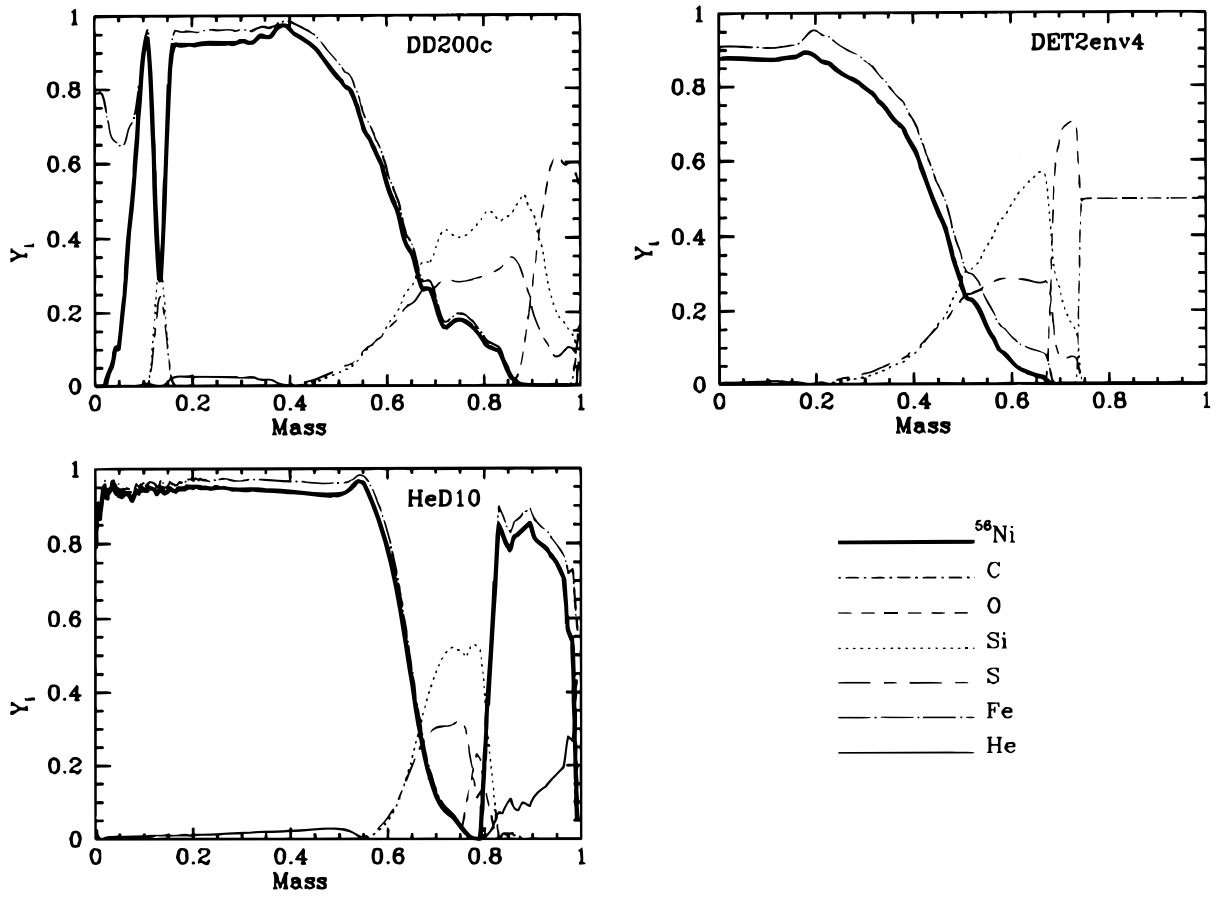

FIG. 1.—Some abundances and ^{56}Ni distribution as a function of mass in stellar units for the delayed detonation model DD200c, the merger model DET2env4, and the helium detonation model HeD10.

Woosley & Weaver (1994), Livne & Arnett (1995), and HK96. This scenario has also been suggested as an explanation of the subluminous SNe Ia (Woosley & Weaver 1994; Ruiz-Lapuente et al. 1993). In this class of models, the thermonuclear runaway starts near the bottom of the outer He layer. The ^{56}Ni distribution (and the subsequent γ-ray emission) differs significantly from the models based on the other scenarios. Because of the large energy release during He burning, $\approx 0.1\ M_\odot$ of ^{56}Ni is produced in the outer region originally composed of helium. Subsequently, a detonation travels inwards and ignites the C-O core at low density, yielding a central concentration of ^{56}Ni at lower velocity. This bimodal ^{56}Ni distribution differs significantly from that expected in the other scenarios (Fig. 1, *bottom*). Depending on model parameters, the amount of this inner ^{56}Ni can be substantial (see model HeD10 in Table 1) and hence represent a potential normally bright SN Ia, or it can be as small as the outer layer, $\approx 0.1\ M_\odot$ (see model HeD6 in Table 1), which could represent a subluminous event.

Basic quantities of the dynamic models are given in Table 1. The quantities given in the data columns are M_*, white dwarf mass; ρ_c, central density (in cgs units) of the white dwarf; α, ratio of deflagration velocity and local sound speed; ρ_{tr}, transition density (cgs units) at which the deflagration is assumed to turn into a detonation; M_{Ni}, mass of synthesized ^{56}Ni. The number in parentheses is the amount of high-velocity ^{56}Ni (Fig. 1). For the helium detonations and the envelope (merger) models, the mass of the C-O core, and the He layers of the hydrostatic white dwarf or of the extended C-O envelope, respectively, are given separately. For all models the initial mass ratio of carbon to oxygen was assumed to be 1 except for model DD203c, for which C-O was assumed to be $\frac{2}{3}$.

The models for delayed detonations, pulsating delayed detonations, and envelope (merger) models are selected from the total array of those models to be the subset with parameters that produce reasonable multicolor light curves of events in the observed sample of both normally bright and subluminous SNe Ia. Calculations of spectral evolution or even maximum light spectra do not yet exist for the whole sample of models, but the selected models are chosen with composition/velocity profiles that are not in obvious disagreement with observations (as are the pure detonation models). For comparison, we note that the structure of the deflagration model W7 (Nomoto, Thielmann, & Yokoi 1984) is similar to that of DD201c. The helium detonation models have been advocated in the literature (Livne & Arnett 1995; Woosley & Weaver 1994; Arnett 1977) as an explanation for both normally bright and subluminous SNe Ia. Sub-Chandrasekhar progenitors would, in principle, be easier to produce from stellar evolution than Chandrasekhar-mass progenitors. There are problems with both the light curves and spectra of this class of models. The light curves are generally too blue (Höflich et al. 1997), and spectra are dominated by Co/Ni. In addition, the normally bright models show excessively weak Si II at maximum light, and the subluminous versions of the model have the Si moving at too low an expansion velocity (Höflich et al. 1997; Nugent et al. 1997). Despite these objections, it is important to investigate this class of models and subject it to observational check in as many ways as possible. As we will argue below, future γ-ray observations can provide a critical check of this class of models.

TABLE 1

PARAMETERS OF DYNAMICAL MODELS OF TYPE Ia SUPERNOVAE

Model	M_* ($M_\odot$)	ρ_c[a] (10^9)	α	ρ_{tr}[a] (10^7)	M_{Ni}[b] ($M_\odot$)
Delayed detonation:					
DD200c	1.4	2.0	0.03	2.0	0.613
DD201c	1.4	2.0	0.03	1.7	0.56
DD202c	1.4	2.0	0.03	2.5	0.67
DD203c[c].....	1.4	2.0	0.03	2.0	0.59
Pulsating delayed:					
PDD5	1.4	2.7	0.03	0.76	0.12
PDD6	1.4	2.7	0.03	2.2	0.56
Helium detonation:					
HeD6	0.6 + 0.172	0.0091	...	...	0.252 (0.08)
HeD10.....	0.8 + 0.22	0.036	...	...	0.75 (0.1)
Detonation + envelope					
DET2env4.....	1.2 + 0.4	0.04	...	...	0.63

[a] In cgs units.
[b] Numbers in parentheses represent the amount of high-velocity ^{56}Ni.
[c] Initial C/O mass ratio assumed to be $\frac{2}{3}$ rather than 1.

4. SPECTRAL EVOLUTION

The evolution of the hard X-ray and γ-ray spectrum of the delayed detonation model DD202c is shown in Figures 2 and 3 (note the changing scale on the vertical axis). The spectrum and its evolution is dominated by nuclear lines and the decay $^{56}\mathrm{Ni} \rightarrow {}^{56}\mathrm{Co} \rightarrow {}^{56}\mathrm{Fe}$, respectively. During the first 2 weeks, ^{56}Ni lines dominate. The continuum is formed by Compton scattering produced by "down" scattered line photons. Below 0.3 MeV (Fig. 3), the spectrum is dominated by the Compton scattering continuum with the exception of a very strong ^{56}Ni line at 0.16 MeV, which can be seen for at least 40 days after the explosion. This line may be observable with a new generation of hard X-ray instruments (see § 5).

After 2 weeks or so, the ^{56}Co lines become the most prominent line features. With increasing time, the Compton optical depth decreases, and eventually the Compton continuum becomes weak (lower panels in Fig. 2). Due to the two- and three-photon decay of ortho- and para-positronium, a strong 511 keV line and a flat continuum below 511 keV are produced. After about 6 weeks, the overall spectral distribution remains unchanged.

The spectral evolution of other evolutionary and dynamical scenarios is shown in Figure 4, which illustrates models PDD6 (a pulsating delayed detonation model that is an alternative for a normally bright SNe Ia) and HeD10 (an example of a bright helium-shell double detonation model). Qualitatively, the profiles look rather similar for all models (including deflagrations like W7; Höflich et al. 1992), with the notable exception of the helium detonations. For the Chandrasekhar-mass or merger models, the model spectra differ mainly at late times, when the ejecta are transparent. At this phase, the central hole in the ^{56}Ni distribution results in flat line profiles. Note the difference between model DD202c in Figure 2 and model PDD6 in Figure 4 at 231 days, where the latter shows a distinct flat top to the lines. These differences give promise of constraints on the central density of the progenitor, the initial deflagration speed, and possibly mixing processes (Höflich et al. 1992). In the absence of gravitation at the center, the flame speed is expected to be close to the laminar deflagration speed and then to accelerate as Rayleigh-Taylor instabilities take over (Khokhlov 1996; Khokhlov et al. 1997a, 1997b; Niemeyer

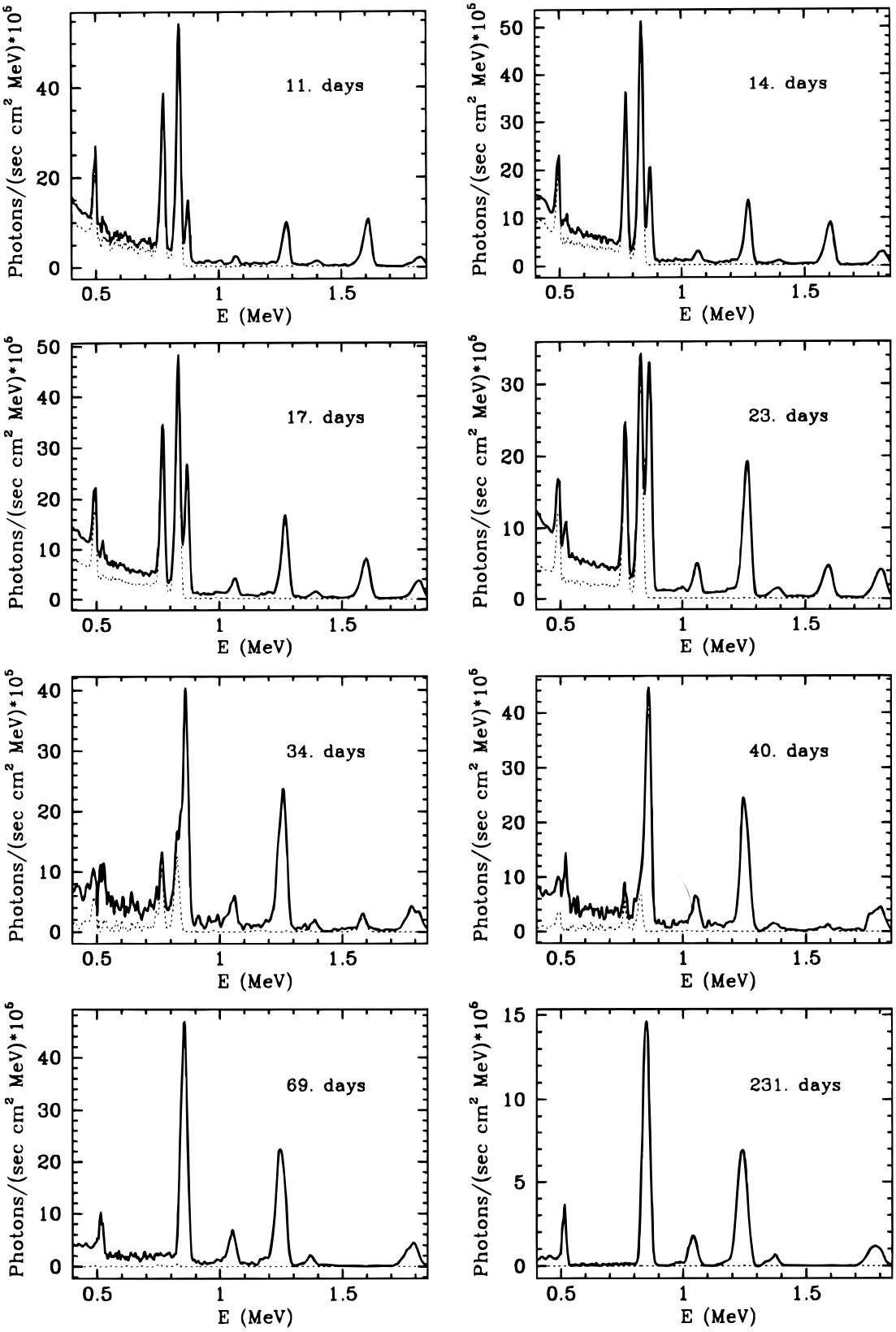

FIG. 2.—Evolution of the γ-ray spectra of the delayed detonation model DD202c. The dashed lines correspond to the contribution of ^{56}Ni. The strongest lines are ^{56}Ni (0.48 MeV), the positron decay line at 0.51 MeV, ^{56}Ni (0.81 MeV), ^{56}Co (0.84 MeV), and ^{56}Co (1.23 MeV).

& Hillebrandt 1995; Niemeyer & Woosley 1997). Late-time γ-ray spectra provide valuable information on the velocity distribution of radioactive material in the expanding envelope, and thus they probe the central density of the white dwarf. To differentiate between different Chandrasekhar-mass and merger models requires high-resolution spectra corresponding to about 1000 km s^{-1}, because the maximum ^{56}Ni velocity varies from about 2000

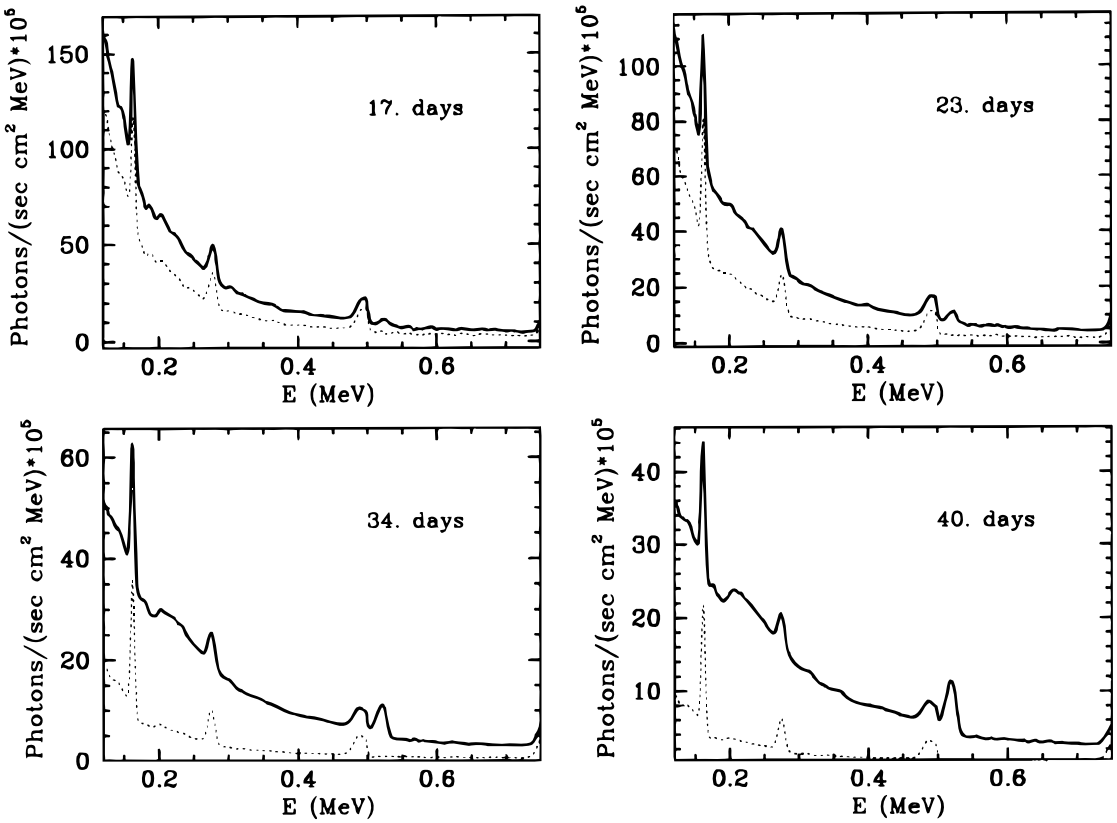

FIG. 3.—Same as Fig. 2, but for lower energies. The strongest lines are the ^{56}Ni lines at 0.158, 0.26, and 0.48 MeV and the positron decay line at 0.51 MeV.

to 3000 km s^{-1} for models that are able to reproduce observations. The ^{56}Ni abundance typically changes by about a factor of 80% over a velocity range of 1000 km s^{-1}. Thus, signal-to-noise ratios of the order of 5 are required to separate the various effects. An alternative, less observationally demanding method is discussed below.

Helium detonations show significantly different γ-ray spectra and spectral evolution compared with the Chandrasekhar-mass and merger models. At all phases, the helium detonation models can thus be distinguished from both Chandrasekhar-mass and merger models with appropriately sensitive observations. The ^{56}Ni at high velocities from the outer detonated helium shell results in very broad profiles beginning a few days after the explosion. Two to 3 weeks after explosion, near or after maximum optical light, the escape probability of γ-rays from the central, low-velocity ^{56}Ni region is sufficient to produce a narrow component atop the broad component (see the panel for model HeD10 at 23 days in Fig. 4). Depending on the total amount of ^{56}Ni, the central component dominates after about 1 month, and eventually a narrow, strongly peaked line remains, with low amplitude but very extended wings. At late times, the amplitude of the high-velocity component is lower than the low-velocity component by almost an order of magnitude, even though the ^{56}Ni mass is lower by a factor of only about 7 in the normally bright model (HeD10) and 3 in the subluminous model (HeD6). The reason is that the outer ^{56}Ni is smeared out over about twice the velocity range, thus diluting the flux at a given energy.

The differences between the Chandrasekhar-mass and sub–Chandrasekhar-mass models are even more defined when the subluminous versions of each are compared. In massive white dwarf models, the mean expansion velocity of the ^{56}Ni decreases with the decrease in total ^{56}Ni mass. This means that the subluminous models that have less nickel according to the dynamical models (Höflich et al. 1995) have narrower lines compared with the models for the normally bright SNe Ia (see also Fig. 7, below). For subluminous helium detonations at early epochs, the ^{56}Ni at high velocities makes the dominant contribution to the flux in a given ^{56}Ni line. Consequently, the ^{56}Ni lines are very broad and nearby lines are blended, unlike the Chandrasekhar-mass models. The mean velocity of the inner ^{56}Ni in the brighter helium detonation model (HeD10 in Fig. 4) is higher than that for the less luminous model (HeD6 in Fig. 5). The velocity profiles of the outer helium layer are similar for the two models. As a result, at late times, the broad "shoulder" remains more visible in the γ-ray spectra of the subluminous helium detonation models, as can be seen by comparing the spectra at 231 days of model HeD10 in Figure 4 with model HeD6 in Figure 5. This "shoulder" in the subluminous models is in especially strong contrast to the late-time line profile of the subluminous Chandrasekhar-mass model, as shown in Figure 5.

In principle, the outer He-^{56}Ni layers of helium detonation models may also be observable in the optical and IR for the first few months, because nonthermal electrons can provide excitation of the corresponding lines (Höflich et al. 1997). In the absence of a magnetic field, the positrons can freely escape after a few months and the optical and IR emission declines. With a tangled magnetic field and a continued trapping of the positrons, this associated optical and IR emission could continue more strongly to later epochs. Early optical and IR spectra may thus provide an addi-

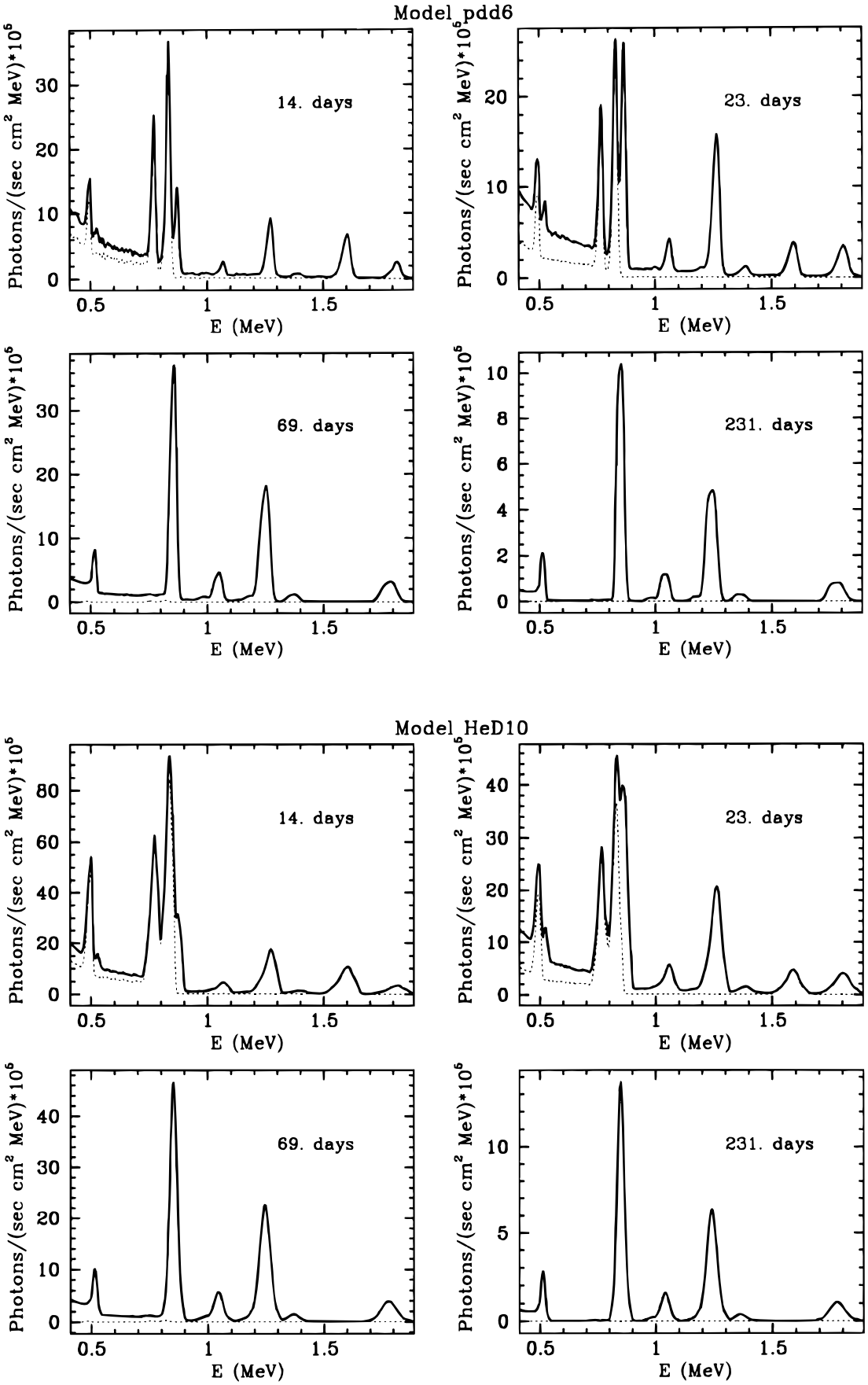

FIG. 4.—Same as Fig. 2, but for the normal bright supernova models PDD6 and HeD10

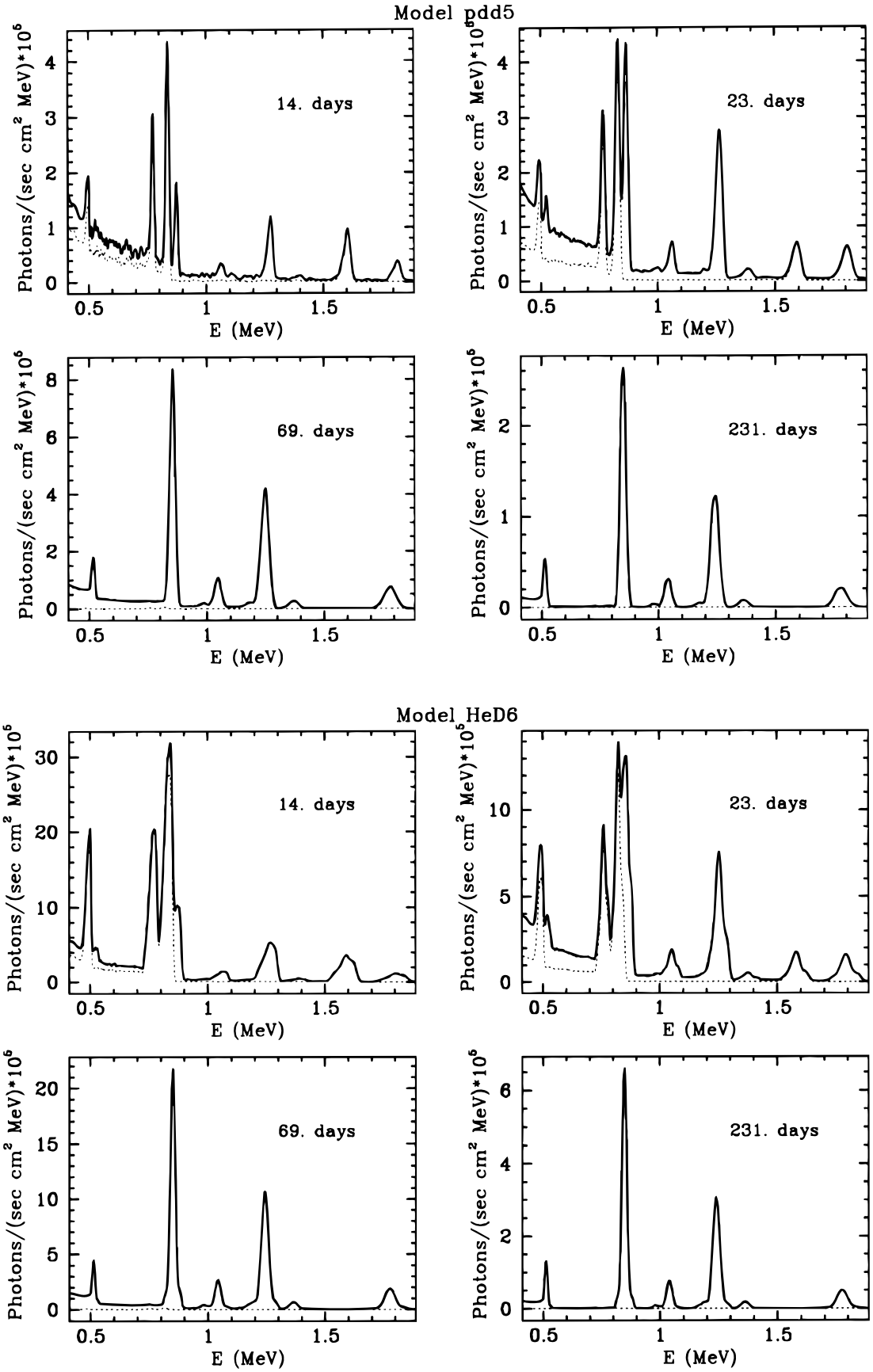

FIG. 5.—Same as Fig. 2, but for the subluminous supernovae models PDD5 and HeD6

tional means to detect the He-^{56}Ni layer, but this possibility is currently controversial. Whereas two groups (Höflich et al. 1997; Nugent et al. 1997) find that helium detonations yield maximum light spectra and light curves that do not reproduce the observations of SNe Ia, Pinto & Eastman (1995, private communication) argue that agreement is possible. Consequently, γ-ray with their straightforward interpretation must be regarded as the best way to ultimately clarify the nature of SNe Ia.

4.1. *Quantitative Analysis of Line Profiles*

In order to provide specific guidance for observational missions, it is appropriate to present more specified detail of the properties of the γ-ray line profiles given in the previous section. Of special importance are the line widths and the displacement of the line with respect to the rest wavelength due to the optical depth and structural effects in the models. The time evolution of the displacement of the line for a variety of models is given in Figure 6 for the two strong lines of ^{56}Co at 0.84 and 1.24 MeV. Figure 7 shows the evolution of the width (FWHM) of the same ^{56}Co lines. Because the Compton cross section decreases slowly with energy and expansion effects dominate, the evolution of the line displacement and width is relatively insensitive to the specific line. Figures 6 and 7 show that the rate of decline of the blueshift of the 0.84 MeV ^{56}Co line is only slightly faster than that of the 1.24 MeV line and that the evolution of the line widths is virtually identical for all models. This common behavior might make it easier to derive constraints from low signal-to-noise data from missions like *CGRO* and *INTEGRAL*. The line shift is critical for a proper analysis of proposed high-sensitivity but narrow wavelength band instruments such as Laue telescopes.

During the first few weeks, the maxima of all γ-ray lines are blueshifted by a velocity that is typically 5000–8000 km s^{-1} with respect to the rest wavelength, because the ejecta

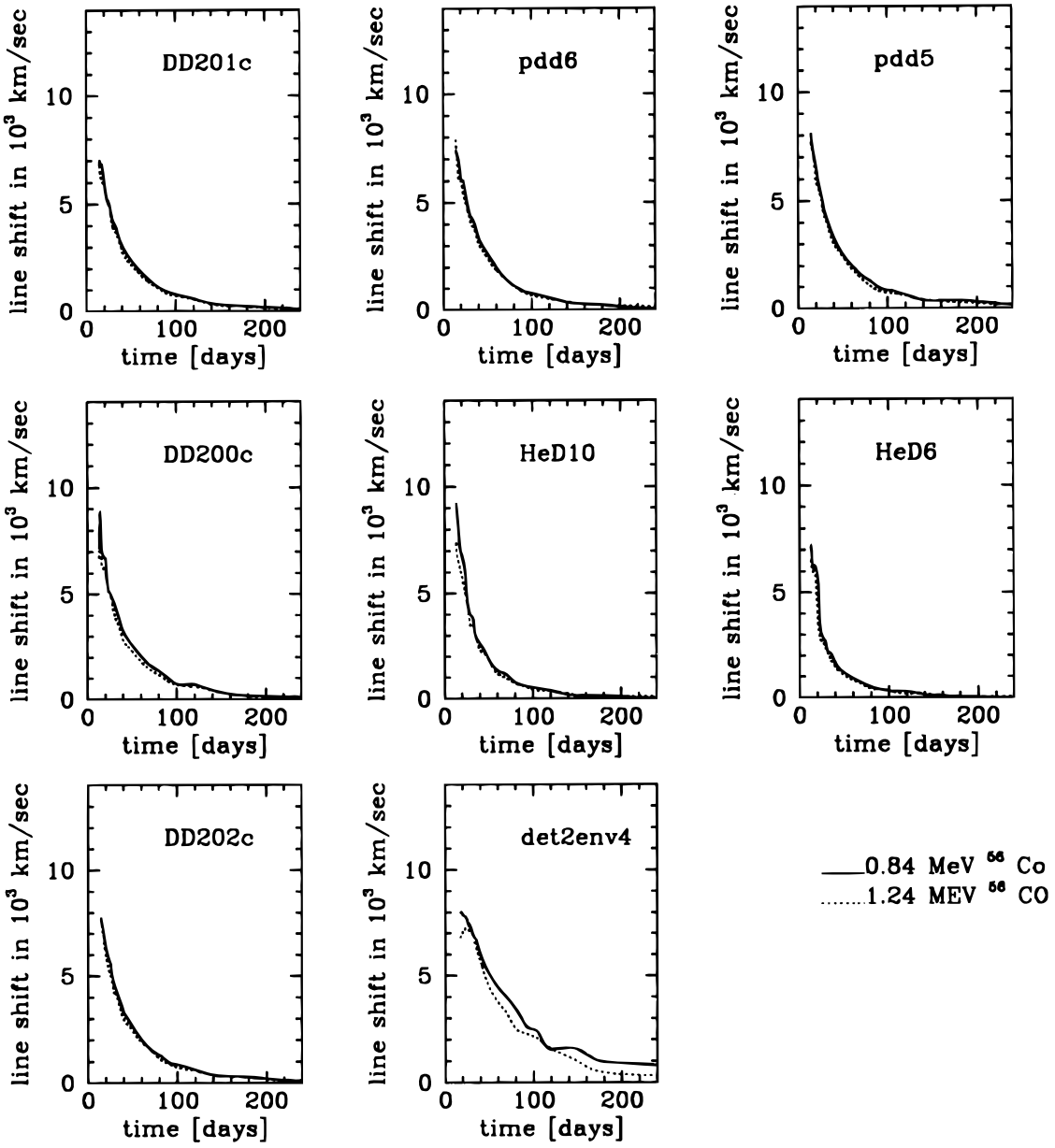

FIG. 6.—Time evolution of the line shift relative to the rest frame. Note that the line shift is insensitive to the specific line considered.

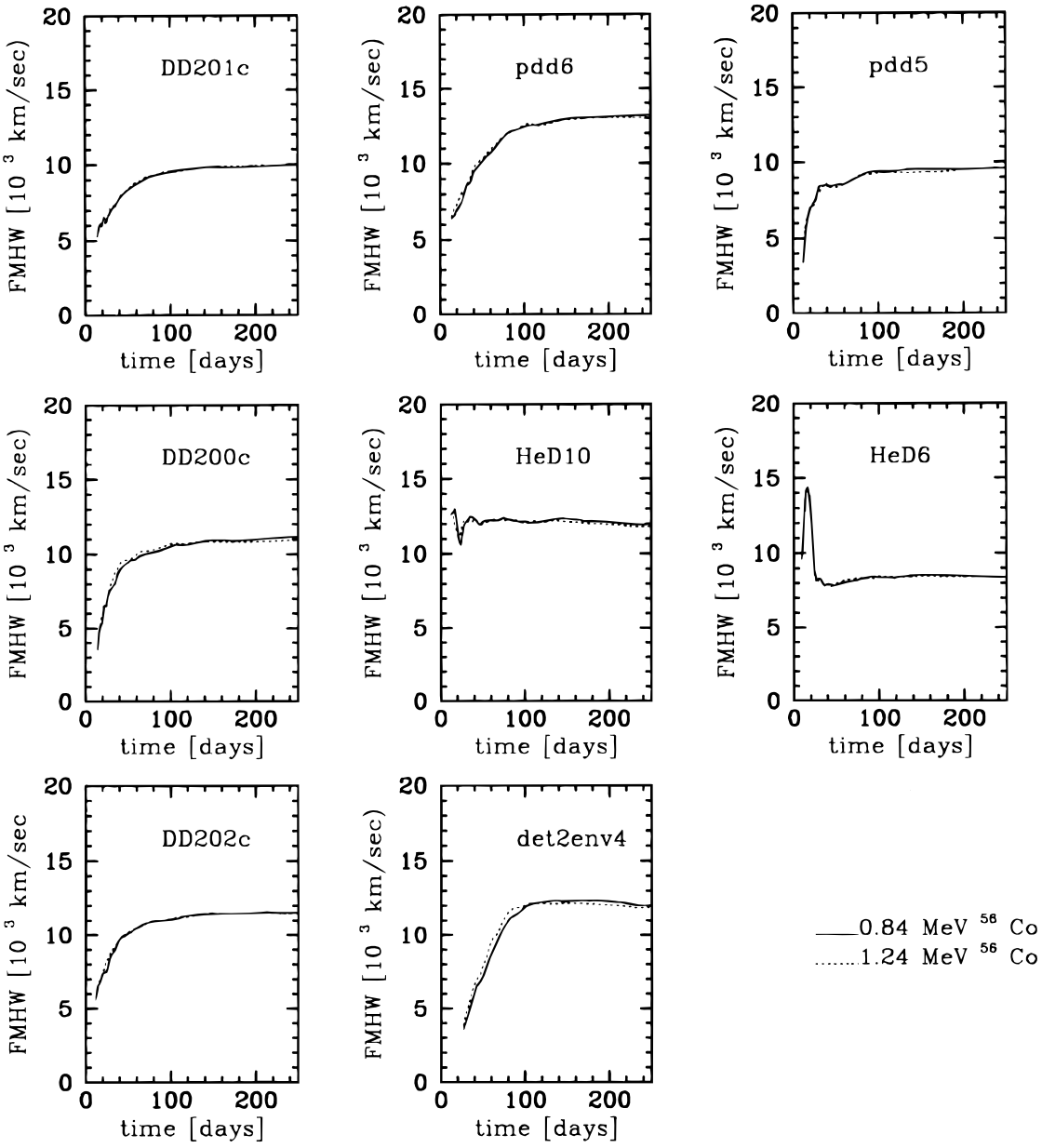

FIG. 7.—Time evolution of the FWHM of the 0.84 and 1.24 MeV ^{56}Co lines. Note that the FWHM is insensitive to the specific line considered.

are optically thick to γ-rays during this epoch and the flux arises from the approaching side. Photons escape essentially radially from the ^{56}Ni region that is expanding toward the observer. The blueshift is comparable to the intrinsic line width, another measure of the kinematic velocity of the radioactive matter. The rate of decrease of the blueshift depends on the optical depth of the ^{56}Ni region and of the matter above it. Consequently, the displacement tends to drop most rapidly with time in the sub-Chandrasekhar models HeD6 and HeD10, and most slowly in the envelope models such as DET2env4 or the pulsating delayed detonations such as PDD6 (see Fig. 6). The evolution of the blueshift during the early epochs (prior to 30 days after the explosion; roughly 2 weeks after optical maximum) might allow discrimination of Chandrasekhar-mass and sub–Chandrasekhar-mass models of the subluminous variety of SNe Ia, as can be seen by comparing the predicted displacement evolution for models PDD5 and HeD6 in Figure 6. With the exception of early-time observations, the line shift is not a powerful discriminant between helium detonation and delayed detonation models. Careful observations of the blueshift over the first 150 days may, however, provide such a test for models with masses larger than M_{Ch}. If observed, a slow evolution of the blueshift could prove the existence of the shell-like structures expected for mergers.

Figure 7 shows that γ-ray line widths can provide detailed discrimination of models for instruments with spectral resolution of order of $\lambda/\delta\lambda \sim 200$–300. Since the line width depends on the velocity distribution of the radioactive material but is insensitive to the wavelength, the results for the 0.84 and 1.24 MeV lines of ^{56}Co given in Figure 7 are quantitatively valid for other lines as well. As shown in Figure 7, the line width for most models increases on timescales of 10–100 days because radioactive material from an increasing velocity range becomes visible as the γ-ray optical depth declines. Since more ^{56}Ni generally implies less shielding by overlying layers and, thus, higher escape probability at early times within each series of models, the

rate of increase of line width is smallest for models with lower ^{56}Ni masses (e.g., DD201c vs. DD202c). For all models, the rate of increase in line width is also smallest for models with "well hidden" ^{56}Ni. This is the case if the model naturally produces a definite shell-like structure such as PDD6, or if the total mass is larger than M_{Ch}, as for the merger models like DET2env4.

The behavior of the sub–Chandrasekhar-mass models with detonating outer helium shells is also conspicuously different in terms of the line width behavior. The lines are very broad beginning soon after the explosion, because of the high expansion velocity of the outer ^{56}Ni produced by the helium detonation. The line width decreases rapidly at about 2 weeks after the explosion. The rapid decline in line width in the helium detonation models can be understood in terms of the line profiles illustrated in Figures 4 and 5 as being due to the increased emission from the narrow inner ^{56}Ni component (see above). With increasing time, this narrow component from the centrally produced ^{56}Ni dominates. The secondary minimum occurs approximately when the monochromatic flux due to the central ^{56}Ni at a low projected velocity dominates the flux of the high-velocity component shifted by 1 Doppler width as the contribution of the high-velocity component becomes insignificant as a result of the larger velocity spread and smaller mass. For normally bright helium detonation models such as HeD10, the central ^{56}Ni mass exceeds that of the outer region by more than a factor of ≈ 7 whereas for subluminous models such as HeD6, this factor is less than 3 (Table 1). Consequently, for subluminous helium detonations, the early spike in the line width is especially pronounced and should be a clear diagnostic for such models.

After about 50 to 150 days, depending on the model, the line widths approach asymptotic values as the envelopes become transparent to γ-rays. In general, the asymptotic value of the FWHM line width corresponds neither to the expansion velocity of the matter within which ^{56}Ni dominates the abundances nor to the mean velocity of the ^{56}Ni. Rather, it measures the projected expansion velocity at which half the amount of radioactive material is located relative to the material seen with zero expansion velocity. For models with centrally concentrated ^{56}Ni, the FWHM depends mainly on the amount of ^{56}Ni and the size of the central hole of the ^{56}Ni distribution. The former can be independently determined by the line flux at late times (see next section). Therefore, the line width provides a unique opportunity to probe the very central region and to obtain insight into the initial conditions at the time of the explosion (see above), namely, the density where the burning starts and the central density of the white dwarf.

5. GAMMA-RAY LINE FLUXES AND LIGHT CURVES

The γ-ray line fluxes and resulting light curves provide another diagnostic to choose among models for the explosion. The information available will depend on whether one knows, from other means, the distance to the source. Figure 8 presents the line-flux light curves for the two strongest lines each of ^{56}Ni and ^{56}Co for a range of relevant models. Figure 9 gives the same information for ^{56}Co, including some of the weaker lines, and Figure 10 does the same for ^{56}Ni.

We first consider the information contained in distance-independent quantities, such as flux ratios. Figure 8 shows that the helium detonation models with radioactive material close to the surface are predicted to have an especially strong line flux at early times. For helium detonation models, the maximum absolute flux due to the ^{56}Ni lines exceeds that of the strongest ^{56}Co lines by about a factor of 5. For all other models, the ^{56}Ni flux remains comparable to or smaller than the flux in ^{56}Co lines. This provides a crucial, distance-independent test for the nature of SNe Ia.

Line-flux ratios for lines of the same radioactive isotope provide a direct measure of the Compton scattering beyond the region containing the radioactive species and thus another way to distinguish different scenarios and to separate explosions of sub–Chandrasekhar-mass and Chandrasekhar-mass progenitors. This is illustrated in Figures 9 and 10. Depending on energy and model, the fluxes of ^{56}Ni lines peak between 10 and 20 days after explosion and those from ^{56}Co peak between 50 and 90 days.

Figures 3 and 9 show that near and after optical maximum, the ^{56}Ni lines at energies below 500 keV have strengths comparable to the strongest γ-ray lines at 0.75 and 0.81 MeV. The positron annihilation line at 0.511 MeV is only moderately weaker than other lines in the MeV range. These results raise the possibility, depending on the sensitivity curve of the instrument, that low-energy ^{56}Ni and the 0.511 MeV lines may be detectable more easily than lines in the MeV range. At early times, all positrons are trapped (Colgate et al. 1997) and so the results do not depend on model-dependent assumptions that would alter the results of positron trapping at later times.

Measurement of line fluxes at both early and late times provides another distance-independent means to test models. Figure 11 presents the ratio R between the total γ-ray luminosity and the total instantaneous energy release by radioactive decay. R measures the transparency of the expanding matter above the region of radioactive elements. It is very model dependent at early times but eventually approaches a value of unity 4–6 months after explosion. Models with high masses and shell-like structrues show small R at early times, whereas the helium detonation models with masses less than M_{Ch} show the highest line ratios.

Besides a comparison of the line strengths of ^{56}Co and ^{56}Ni, the change of the line ratios provides important information on the structure of the envelope. This constraint comes by comparing lines at different energies as illustrated in Figure 12, which presents results for the 1.24 and 0.84 MeV lines of ^{56}Co for a range of models. By comparing critical line ratios with their asymptotic values, the Compton depth can be constrained. Figure 12 shows that the ^{56}Co line ratio is sensitive to both time and the model. The line ratios depend mainly on the amount of material above the radioactive layer; however, self-shielding within the radioactive region is also important. At early epochs, even the helium detonation models with their exposed outer layers of ^{56}Ni show line ratios that substantially exceed the asymptotic value (Fig. 12). Observations during the first 2–3 months are most suitable in this regard. To distinguish helium detonation models from the merger scenario and the explosion of massive white dwarfs, the line ratios must be known to better than $\approx 20\%$. Note that late-time observations are not actually required, because the asymptotic value is fixed by the branching ratio.

Other constraints on the models are possible in the case where the distance is known from, e.g., δ Cepheids (Saha et al. 1996; Freedman et al. 1994) or from optical light curves

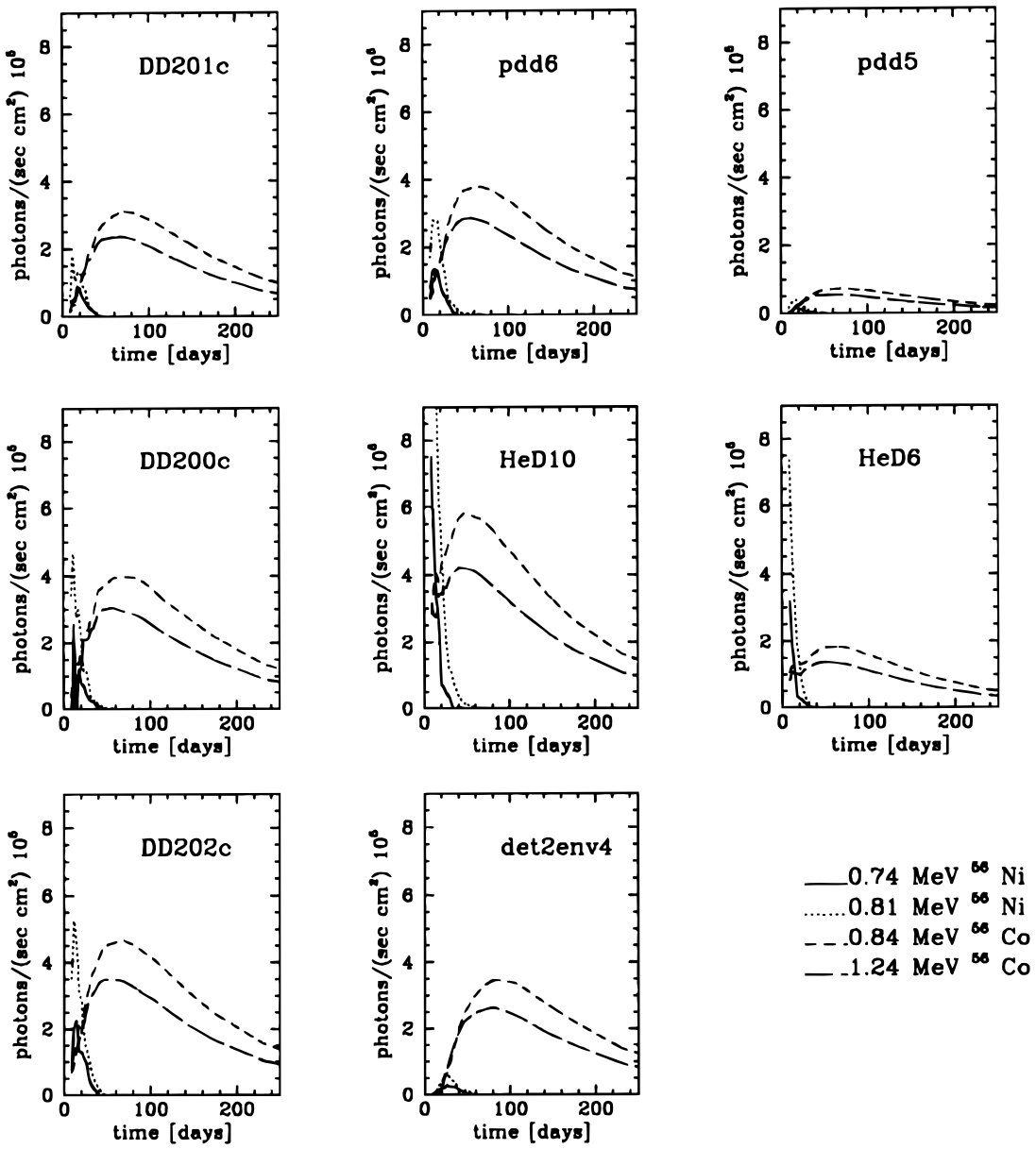

FIG. 8.—Time evolution of the integrated line fluxes of the most prominent γ-ray lines of ^{56}Ni and ^{56}Co as predicted by theoretical models (see Table 1) assuming a distance of 10 Mpc.

and spectra (e.g., Hamuy et al. 1996; HK96; Riess et al. 1996). In this case, models can be distinguished by the time evolution of absolute line fluxes, as illustrated in Figures 8, 9, and 10. For the helium detonation models, the flux in the strongest ^{56}Ni lines should be in excess of 10^5 photons s^{-1} cm^{-2} if observed at a distance of 10 Mpc as the flux peaks between 10 and 20 days after the explosion. Late-time measurements would allow the determination of the absolute amount of radioactive material for given distance.

5.1. *Determination of the Time of the Explosion*

The early, rapid change of the spectra may allow an accurate measure of the time of the explosion (Clayton et al. 1969). Photons at similar energies encounter the same degradation due to Compton scattering, and thus the time-dependent flux ratio of the lines of similar energy does not depend on the model, as shown in Figure 13. Two spectral regions are especially suitable for determining the time of explosion: that at about 0.8 containing the 0.81 MeV line of ^{56}Ni and the ^{56}Co line at 0.84 MeV, and that near 0.5 MeV containing the positron annihilation line at 0.511 MeV and the ^{56}Ni line at 0.48 MeV (Figs. 2 and 3). Figure 13 shows the ratio of the 0.81 MeV line of ^{56}Ni in comparison with the 0.84 MeV line of ^{56}Co. The ratio of the 0.48 MeV line to that at 0.511 MeV follows an essentially identical trajectory, but with an amplitude decreased by a factor of 3.5. The ratio of the ^{56}Ni to ^{56}Co lines at 0.8 MeV has the advantage of involving strong lines with a large flux ratio, but its use is restricted to times between approximately 11 and 25 days without being obscured by contributions of Compton-scattered photons of the ^{56}Co line. The ratio of the ^{56}Ni line to the annihilation line at 0.5 MeV is based on lines with more moderate fluxes, but in principle, it can be used between days 20 and 50 for nearby SNe Ia.

5.2. *Effect of Integration Times*

Integration times for γ-ray lines may be on the order of days to weeks. Therefore, it is useful to characterize the

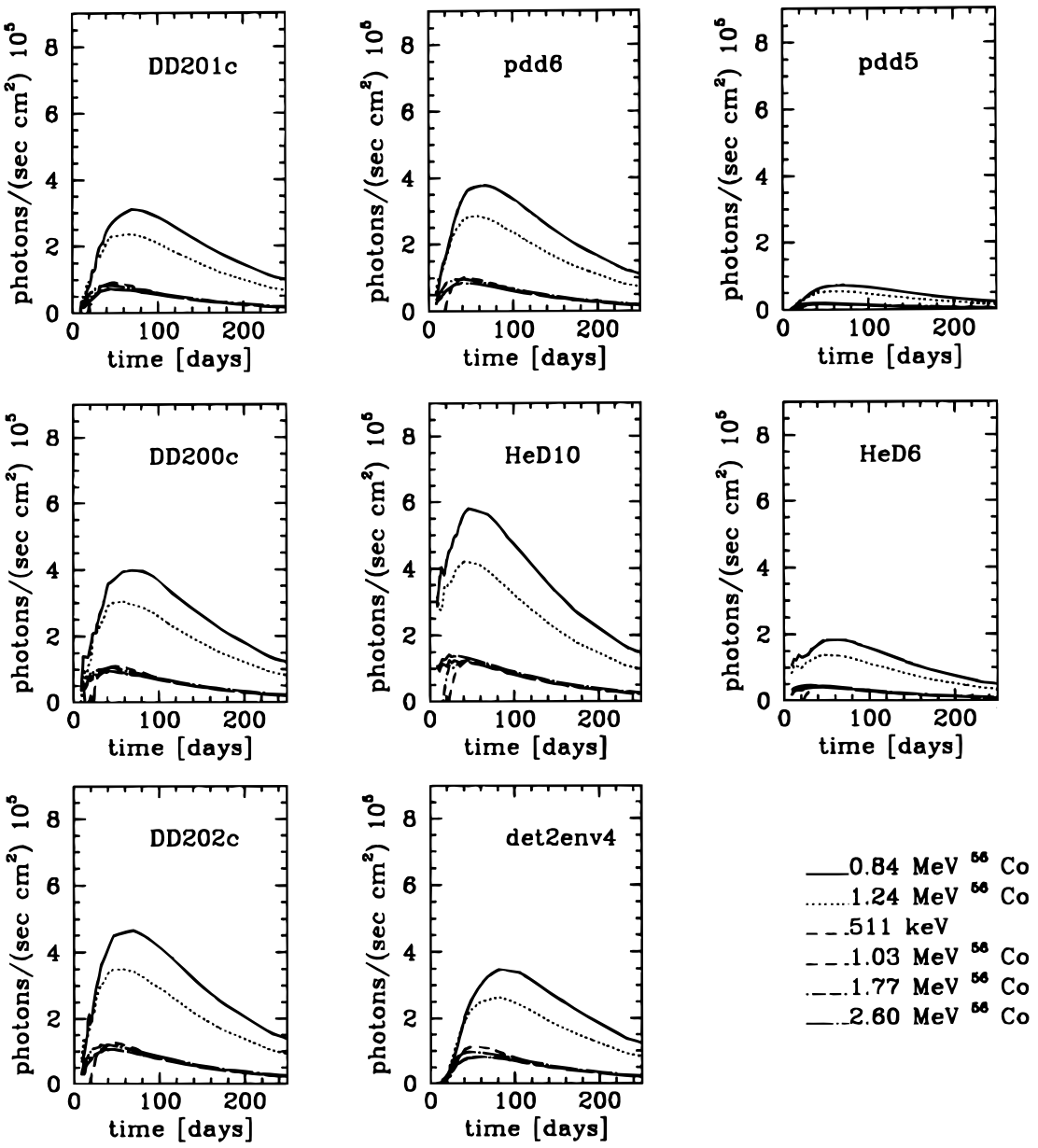

FIG. 9.—Same as Fig. 8, for ^{56}Co, but including weaker lines

influence of the integration time on the resulting spectrum, which depends on both the mean time and the underlying model. The model dependence enters because the time evolution of the absolute fluxes determines the weighting of the line fluxes over the observed time interval.

Figure 14 illustrates the change of the spectrum with integration time for the specific example of the delayed detonation model DD201c at about 14 and 23 days after the explosion. For $\Delta t < 10$ days, the resulting error in the line flux remains smaller than 10% for the Chandrasekhar-mass and merger models. The moderate size of the error is due to the rather small changes in the absolute fluxes compared with the time-averaged spectra (Figs. 1–5). For the helium detonation models, the situation is different. For this class of models, the large early fluxes and rapid change with time (e.g., by a factor of 2 between days 14 and 23; Fig. 4) demand integration times less than ≈ 5 days to achieve the same error level of less than 10%. This should not pose a serious problem, because the high γ-ray fluxes expected from the helium detonation models would allow shorter integration times. Note that the error in the time of the explosion can be further reduced if information about the time evolution of the absolute flux can be determined directly by γ-ray observations or, alternatively, by using restrictions on the model derived by the many constraints outlined in previous sections.

6. SUPERNOVA DETECTION RATE

The largest obstacle to γ-ray astronomy of supernovae is achieving sufficient sensitivity. This directly affects the observability of SNe Ia with the current generation of γ-observatories, i.e., *CGRO*, the upcoming *INTEGRAL* mission, and the proposed third generation of instruments including Compton and Laue telescopes. The sensitivity of the instruments generally increases for intrinsically narrower lines. Since the supernova features tend to be narrower at early epochs (Fig. 7), early-time observations are highly favored for the detection of γ-ray lines.

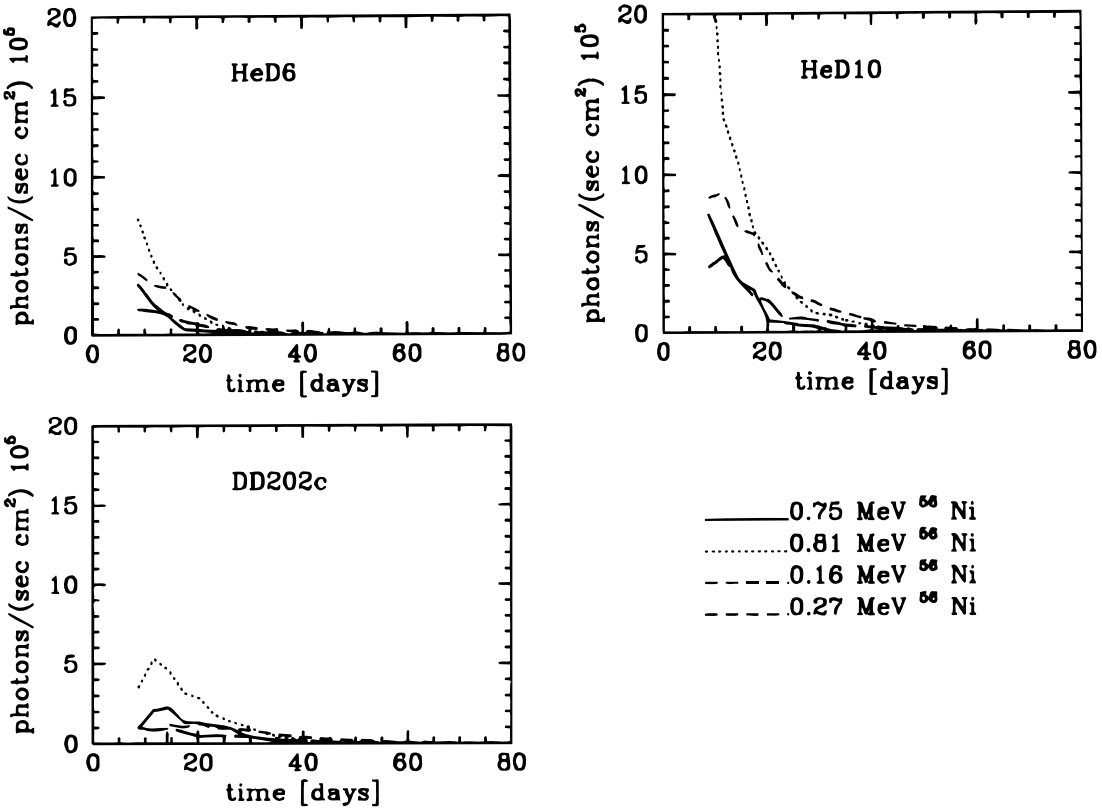

FIG. 10.—Same as Fig. 8, but for ^{56}Ni

The detection limits, $F_{\min}$, depend on the mission and instrument. For the instruments on *CGRO* (i.e., COMPTEL and OSSE), $F_{\min} = 10^{-4.5}$ photons s^{-1} cm^{-2} at about 1 MeV (Johnson et al. 1993). This limit will unfortunately degrade to about $10^{-4.1}$ photons s^{-1} cm^{-2} after the orbit boost that is planned as this paper is written. According to its design parameters, the goal of *INTEGRAL* was to reach $F_{\min} = 10^{-5.5}$ photons s^{-1} cm^{-2} (von Ballmoos, Dean, & Winkler 1995). Recent tests have, however, suggested that this limit must be revised upward. Assuming an integration time of 10^6 s and a 3 σ detection, the line sensitivities are $10^{-4.7}$ and $10^{-4.3}$ photons s^{-1} cm^{-2} for a line width $\delta E/E$ of 1% and 10%, respectively. For the classical γ-ray lines of ^{56}Co at 0.84 and 1.24 MeV, the sensitivity will only be comparable to COMPTEL (Matteson 1977). Sensitivities larger by a factor of 2–3 can be achieved at energies of $\sim$100–700 keV. The continuum sensitivity ranges from about 10^{-6} photons s^{-1} cm^{-2} MeV^{-1} at 100 keV to $10^{-7.3}$ photons s^{-1} cm^{-2} MeV^{-1} at about 1 MeV.

The third generation of proposed γ-ray instruments are likely to use either the Compton effect or Laue refraction. The first type of instrument reproduces the well-proven technology of COMPTEL. The second type uses the new technology of focusing lenses. The advantage of the first type is a wide energy range that makes it the ideal multipurpose instrument. The disadvantage is its size, which exacerbates problems of both background reduction and cost. Laue telescopes can, in principle, overcome both these disadvantages because of their compactness. Such instruments are, however, only able to cover a very narrow energy range comparable to the intrinsic line widths predicted for supernovae. Thus they can detect only one line feature at a time. Currently, the Laue instruments must be regarded as an option to study individual selected lines. For both types

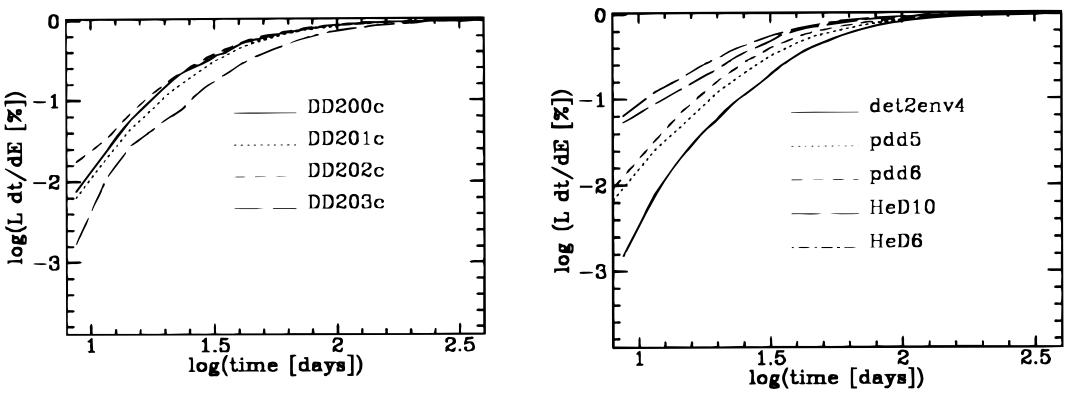

FIG. 11.—Luminosity above 10 keV relative to the energy production by radioactive decays

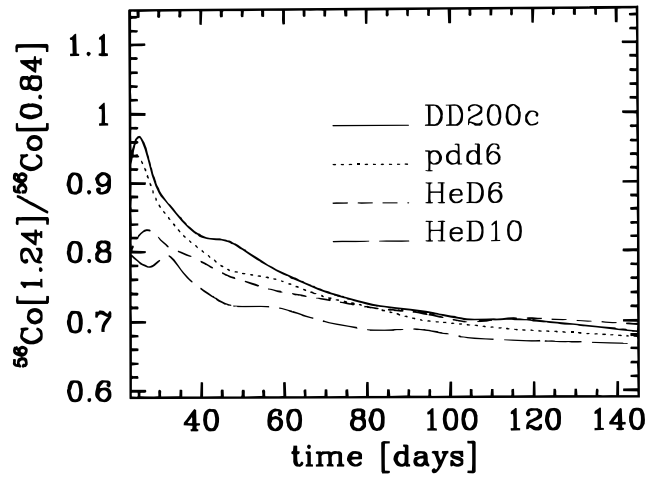

FIG. 12.—Ratio between the ^{56}Co 1.24 and 0.84 MeV lines. This ratio depends sensitively on the model.

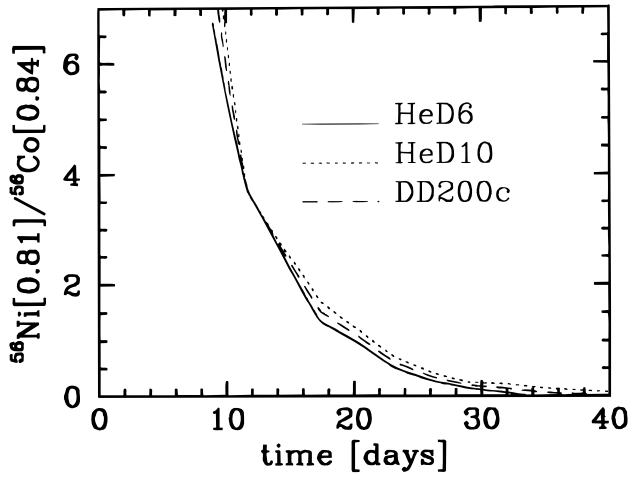

FIG. 13.—Ratio between the ^{56}Ni 0.81 MeV and ^{56}Co 0.84 MeV lines. This ratio depends sensitively on the time after the explosion, but it hardly depends on the model. The line ratio between the 0.48 MeV ^{56}Ni and the 511 keV positron annihilation lines is 3.5.

of instruments, the realistic design goals are a broad line sensitivity of the order of 10^{-6} photons s^{-1} cm^{-2} (J. D. Kurfess 1997, private communication), substantially more sensitive than *CGRO* or *INTEGRAL*.

The observability of supernovae depends on both the rate of occurrence of events and their distance. In recent years, the number of supernovae discovered nearby has been rather constant, suggesting that essentially all nearby supernovae that could be targets for γ-ray spectroscopy are being discovered. Table 2 gives the number of SNe Ia discovered in 1991 and 1992 based on the Asiago catalog. Only a small fraction of these events have been analyzed in detail; however, most SNe Ia are of similar brightness, comparable to normally bright SNe Ia. From recent studies, the mean absolute magnitude at maximum in V is approximately -19.3 mag with a spread of about 0.4 mag (e.g., Hamuy et al. 1996; HK96). Statistically, the absolute brightness can be translated into an estimate of distances to individual observed SNe Ia as presented in Table 2.

From the general properties of observed supernovae and the light curves and spectra of individual events, the delayed detonation and pulsating delayed detonation models seem to be the most promising ones to account for the majority of SNe Ia events (see, e.g., Höflich et al. 1997 and references therein). Therefore, we have chosen the delayed detonation model DD201c to provide a guideline for the observability

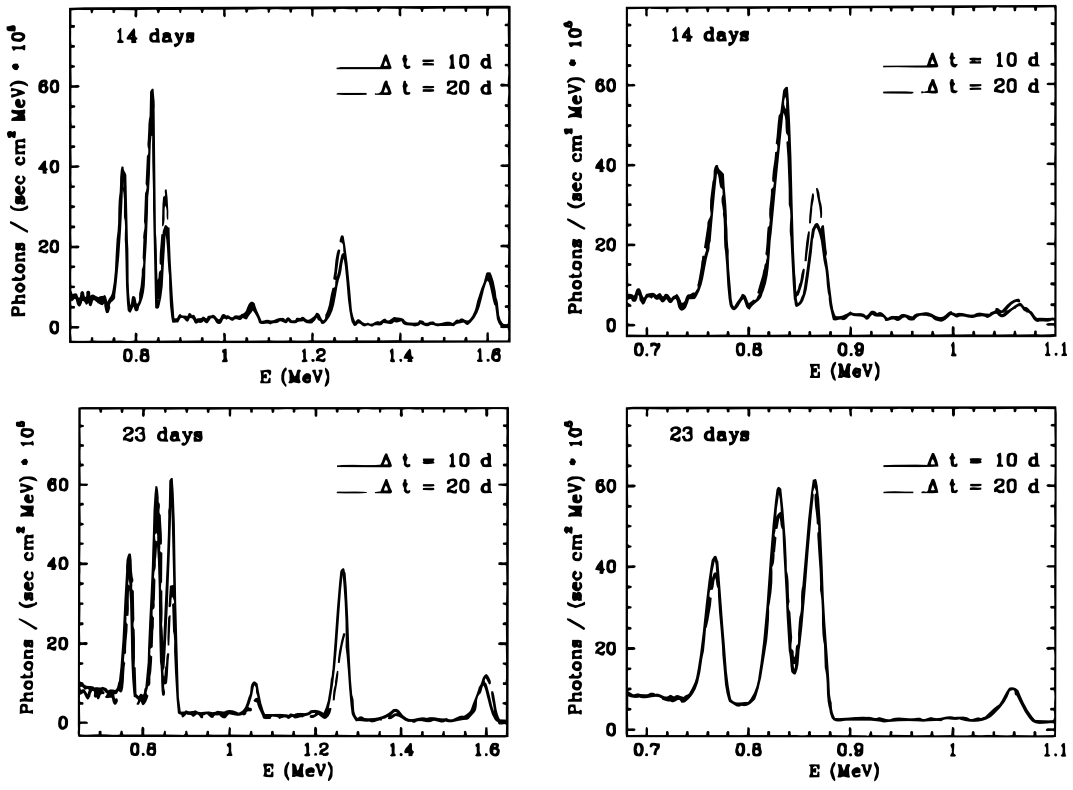

FIG. 14.—Predicted spectrum as a function of integration times around days 14 and 23 for the delayed detonation model DD201c

TABLE 2

TYPE Ia SUPERNOVA RATE AS A FUNCTION OF DISTANCE

MAXIMUM V BRIGHTNESS	DISCOVERED (1991–1992)	EXPECTED	DISTANCE (Mpc)	FLUX (photons s^{-1} cm^{-2})	
				$t = 70$ days	$t = 180$ days
10.0	0	0.02	7.24	8.6E − 05	4.8E − 05
10.5	0	0.02	9.12	5.4E − 05	3.0E − 05
11.0	0	0.07	11.48	3.4E − 05	1.9E − 05
11.5	0	0.12	14.45	2.2E − 05	1.2E − 05
12.0	1	0.26	18.20	1.4E − 05	7.5E − 06
12.5	0	0.50	22.91	8.6E − 06	4.8E − 06
13.0	0	1.01	28.84	5.4E − 06	3.0E − 06
13.5	3	2.00	36.31	3.4E − 06	1.9E − 06
14.0	2	4.00	45.71	2.2E − 06	1.2E − 06
14.5	1	7.97	57.54	1.4E − 06	7.5E − 07
15.0	3	15.92	72.44	8.6E − 07	4.8E − 07
15.5	1	31.74	91.20	5.4E − 07	3.0E − 07
16.0	5	63.35	114.82	3.4E − 07	1.9E − 07
16.5	6	126.37	144.54	2.2E − 07	1.2E − 07
17.0	4	252.17	181.97	1.4E − 07	7.5E − 08
17.5	6	503.12	229.09	8.6E − 08	4.8E − 08
18.0	24	1003.89	288.40	5.4E − 08	3.0E − 08

of SNe Ia in γ-ray lines. For all models of normally bright events, the maximum γ-ray flux varies only within $\approx 50\%$ (see Fig. 8). Since the flux scales inversely with the distance, that effect will dominate and our particular choice of model does not substantially affect this discussion. For SNe Ia at the luminous end of the observed luminosity distribution, distances up to which a detection may be possible should be scaled up by, at most, 50%.

For *CGRO*, after the orbit boost with a detectability limit of $F_{\min} \simeq 10^{-4.1}$ photons s^{-1} cm^{-2}, Table 2 shows that normally bright SNe Ia will be detectable up to a distance of 7 Mpc with an upper limit of about 10 Mpc. Statistically, there is an SNe Ia at a distance between 4 and 9 Mpc about once every 8 years (e.g., 4.6 Mpc for SN 1972e, 4.5 Mpc for SN 1986g, 8.4 Mpc for SN 1989b), somewhat higher than the simple estimate of Table 2. Such an event would clearly allow for a positive measurement of the γ-ray fluxes or would rule out all the present models. Because of the long expected operational time of *CGRO* (≥ 10 yr), there is a good chance that a clear detection of ^{56}Co lines could be obtained, which would allow different models within each explosion scenario to be distinguished. The low energy resolution of *CGRO* would not permit the use of information on the velocity distribution. If, however, the relative fluxes of, e.g., the 0.84 and 1.24 MeV lines could be measured to within an accuracy of 10% and observations are available up to 50 days after the explosion, the line ratios would provide a distinction between the explosion of a massive white dwarf and that of a sub-Chandrasekhar helium detonation.

A much cleaner distinction between Chandrasekhar and sub-Chandrasekhar models could be achieved if observations were available at early epochs, about 15 to 20 days after the explosion, corresponding to about maximum visual light. Several SNe Ia have been discovered up to about 2 weeks before maximum (see, e.g., Hamuy et al. 1996 for a list), so γ-ray observations at these times may not be unrealistic. Figure 10 shows that the peak ^{56}Ni flux of the sub-Chandrasekhar models exceed that of the Chandrasekhar-mass models by a factor of 5 for normally bright models about 10 days after the explosion and by factors of several at later epochs. At 10 days after the explosion, the normally bright helium detonation models predict a flux of $\approx 2 \times 10^{-4}$ photons s^{-1} cm^{-2} at 10 Mpc, and at maximum light, ≈ 15 days after the explosion, a flux of $\approx 10^{-4}$ photons s^{-1} cm^{-2}, factors of about 5 and 2, respectively, brighter than predicted at 70 days. Given the high maximum ^{56}Ni line fluxes of helium detonation models, both normally bright and subluminous Type Ia should be detectable by *CGRO* up to distances of 15 and 10 Mpc, respectively, if the observations start about 1 week before maximum light in the optical wavelength range, or these scenarios can be ruled out. SNe Ia within 15 Mpc occur about once every 5–10 years. In particular, the helium detonation scenario predicts the detectability by *CGRO* of all normally bright SNe Ia before optical maximum in the Virgo Cluster, at about 18–20 Mpc, where an SN Ia should have an apparent magnitude of $V = 12$–12.5. Based on Table 2, the opportunity for such an observation might be available every 3 to 4 years as supernova searches of all kinds become more successful at discovering SNe Ia well before maximum light. In particular, SN 1991T would have provided a rigorous test of the helium detonation models had the *CGRO* observations been made at a sufficiently early epoch. The key point is thus if an appropriately early *CGRO* observation significantly fails to detect a flux of $\approx 5 \times 10^{-5}$ photons s^{-1} cm^{-2} from an SN Ia of $V = 12.5$, then helium detonation models can be ruled out. A detection or even a firm upper limit for any SNe Ia in the Virgo Cluster will provide a much needed distinction between Chandrasekhar and sub-Chandrasekhar models.

With *INTEGRAL*, the next-generation γ-ray observatory, all the types of observations discussed here are feasible for the classical strong ^{56}Co lines that have been discussed in the context of *CGRO*. In addition, the high velocity resolution (≈ 600 km s^{-1}; Matteson 1997) will allow detailed studies of line profiles (see above). An especially exciting possibility arises from the high sensitivity at low energies and the low energy threshold of *INTEGRAL*, which will allow detections of both the 0.511 MeV line of positronium and the ^{56}Ni line at 0.48 MeV. Although the corresponding lines are weaker by a factor of 4 compared with the strongest lines of ^{56}Ni and ^{56}Co, the increased low-energy sensitivity of *INTEGRAL* should allow detec-

tion of the positron decay line up to about 10–13 Mpc for normally bright SNe Ia over a period of several months. Observations during the first month after explosion would allow detailed studies of ^{56}Ni lines and the 0.511 MeV line and, consequently, would provide for the first time a realistic way to determine the time of the explosion (Fig. 13). With *INTEGRAL*, the very strong ^{56}Ni lines at about 0.16 and 0.27 MeV and the Compton continuum can be detected (Fig. 1) out to distances including the near side of the Virgo Cluster. Therefore, a target of opportunity could be expected every 3 to 4 years.

For the third-generation instruments, all SNe Ia within a distance of 70–100 Mpc would be within reach. This translates into about six targets of opportunity per year. Detailed studies of a variety of supernovae including their statistical properties would be possible. All the effects mentioned in the previous sections could be studied in great detail, opening a new window to perform γ-ray astronomy of supernovae on a regular basis.

The sensitivity of the proposed third-generation experiments brings an entirely new aspect to γ-ray astronomy of supernovae. Up to this point, the current discussion has been based on the premise that all supernovae to be studied will be discovered by standard ground-based optical search techniques. The record of distant supernovae discovered in this way must be very incomplete. As can be seen from Table 2, the number of discoveries does not scale with the volume, even for distances not affected by clustering. This strongly suggests the presence of selection effects, which must depend on the type of the host galaxy, the extinction, and the distance from the center of the galaxy. These questions are highly relevant to clarify the progenitor population and its influence on the rate of discovery and nature of the supernovae. These issues have important consequences for the use of SNe Ia to obtain extragalactic distances at high redshift (Höflich et al. 1997).

7. POSITRON TRAPPING

One of the more interesting and still unsolved problems of SNe Ia is the physics that determines the slope of the late-time light curve. As emphasized by Colgate (Colgate, Petschek, & Kriese 1980; Colgate 1983; Colgate et al. 1997), the exponential decay continues for many *e*-folds, in excess of 600 days (Kirshner et al. 1993). There is no observational evidence for the decline of the optical light curve because of an "infrared catastrophe" (Weaver, Axelrod, & Woosley 1980) that is predicted to occur as standard thermonuclear models expand and cool. With assumed complete trapping of positrons due to tangled magnetic fields and the resulting small Larmor radii, the line emission shifts to the IR fine-structure lines of iron. Colgate has argued that this problem requires a complete shift of paradigm and is in favor of a model based on core collapse that ejects only a small amount of highly nickel-enriched matter ($\sim 0.4\ M_\odot$). He further proposes that with the small mass and associated radial combing of the magnetic field, the positrons would leak out with a deposition function that is essentially self-similar to that for γ-rays. Colgate argues that the resulting deposited power in positrons could be restricted to optical emission through fluorescence effects and could then produce the observed long-time exponential decay. This model is very unlikely to apply to SNe Ia since it would yield spectra anomalously rich in ^{56}Ni and poor in intermediate-mass elements, continua that are too blue (for the same reasons as the helium detonation models), excessively high velocities, light curves that peak and decline too rapidly, and implied distances that are incommensurate with those determined by δ Cepheids. Nevertheless, Colgate is right that the problem of the late-time decay must be solved in the context of the thermonuclear models before they can be regarded as complete. Gamma-ray observations should help to clarify this important issue of physics.

To constrain positron trapping, late-time observations are necessary. Even with no magnetic field, positrons are not predicted to begin leaking, thereby reducing the positron energy deposition function, until about 300 days. The flux is correspondingly small at this time. *INTEGRAL* would require a supernova within only a few megaparsecs to make the corresponding detection. The next generation of γ-ray telescopes could, however, make a substantial contribution to this issue. A flux limit of 10^{-6} photons s^{-1} cm^{-2} would allow a measurement of the difference in the positron flux between fully trapped and freely leaking models for supernovae out to the Virgo Cluster.

The issue of the positron leakage could be approached in several ways, some of which might be distance dependent and some of which would require an independent measure of the distance. One method would be to look carefully at the 0.511 MeV line flux, in an absolute sense, or in comparison with the ^{56}Co lines at the same epoch. Another technique, which would not require narrow line resolution, would be to look at the absolute or relative photon flux of the positronium continuum. Because the photon flux is constant, it may even be detectable as a constant contribution to the X-ray flux by X-ray instruments as a result of their superior sensitivity.

8. DISCUSSION AND CONCLUSIONS

We have presented γ-ray spectra and light curves for a variety of models of SNe Ia, including delayed detonation, pulsating delayed detonations, merger scenarios, and helium detonations. Gamma rays trace the radioactive isotopes whereas optical photons trace elements; therefore, γ-ray observations must be seen as an important complement to those at other wavelengths.

A detailed discussion of the properties of the emitted spectra were given. These properties provide sensitive tools to study details of the explosion models and information that is relevant for the data analysis of the γ-ray observations themselves. Since the different model scenarios show very different signatures in their time evolution, spectral features, and line ratios, observation of γ-rays has the capacity to remove any ambiguity about the basic nature of SNe Ia, whether they involve thermonuclear explosion or core collapse (and, in the expected former case, whether they involve Chandrasekhar-mass or sub–Chandrasekhar-mass white dwarfs). For nearby supernovae, γ-ray spectroscopy has the potential to separate effects due to the initial metallicity of the exploding white dwarf, mixing, and nuclear burning.

A comparison of γ-ray fluxes and bolometric (UV/optical/IR) light curves can provide a measure of the escape probability of positrons and, in principle, of the magnetic field strength and distribution. Gamma rays provide an unbiased, direct tool to test the calibration of SNe Ia and to overcome systematic effects due to reddening and errors in the calibration of secondary distance indicators. Such tests are critical for the future use of SNe Ia as distance indica-

tors to determine the deceleration parameter and other cosmologically relevant parameters.

SNe Ia are not a strictly homogeneous group of objects, as previously believed. Therefore, any study of them must include a large number of events. For γ-ray astronomy, this implies that a broad-line sensitivity of about 10^{-6} photons s^{-1} cm^{-2} is needed to bring within reach all SNe Ia up to a distance of 70–100 Mpc. Based on current discovery rates in the optical region, this translates into about 6–8 SN yr^{-1}, each of which would be detectable for a period of about 6 months.

The increased sensitivity of future generations of instruments will give for the first time the absolute and relative rates of SNe Ia as functions of galaxy type, unbiased by extinction and the type of the host galaxy, which, as can be seen from Table 2, hampers optical searches. A monitoring of distant clusters on a regular basis is feasible because an entire cluster can be observed simultaneously, given the wide field of view of γ-ray detectors. This should provide valuable information on the progenitor evolution, still one of the major mysteries associated with SNe Ia.

P. A. H. thanks J. D. Kurfess for the organization of the excellent workshop on gamma-ray astrophysics in Washington and all participants for the interesting discussions. This research was supported in part by NSF grant AST 95-28110, NASA grant NAG 5-2888, and a grant from the Texas Advanced Research Program.

REFERENCES

Ambwani, K., & Sutherland, P. G. 1988, ApJ, 325, 820
Arnett, D. 1997, in Thermonuclear Supernovae, ed. P. Ruiz-Lapuente, R. Canal, & J. Isern (NATO ASI Ser. C, 486) (Dordrecht: Kluwer), 405
Benz, W., Bowers, R. L., Cameron, A. G. W., & Press, W. H. 1990, ApJ, 348, 647
Burrows, A., Shankar, A., & Van Riper, K. A. 1991, ApJ, 379, L7
Burrows, A., & The, L.-H. 1990, ApJ, 360, 626
Chan, K. W., & Lingenfelter, R. E. 1988, in AIP Conf. Proc. 170, Nuclear Spectroscopy of Astrophysical Sources, ed. N. Gehrels & G. Share (New York: AIP), 110
———. 1990, Proc. 21st Int. Cosmic Ray Conference (Adelaide), 1, 101
———. 1991, ApJ, 368, 515
Clayton, D. D. 1974, ApJ, 188, 155
Clayton, D. D., Colgate, S. A., & Fishman, G. J. 1969, ApJ, 155, 75
Colgate, S. A. 1983, in AIP Conf. Proc. 101, Positron-Electron Pairs in Astrophysics, ed. M. D. Greenbelt (New York: AIP), 94
Colgate, S. A., Fryer, C. L., & Hand, K. P. 1997, in Thermonuclear Supernovae, ed. P. Ruiz-Lapuente, R. Canal, & J. Isern (NATO ASI Ser. C, 486) (Dordrecht: Kluwer), 273
Colgate, S. A., Petschek, A. G., & Kriese, J. T. 1980, ApJ, 237, L81
Collela, P., & Woodward, P. R. 1984, J. Comput. Phys., 54, 174
Freedman, W. L., et al. 1994, ApJ, 427, 628
Hamuy, M., Phillips, M. M., Suntzeff, N. B., Schommer, R. A., Maza, J., Smith, R. C., Lird, P., & Avilés, R. 1996, AJ, 112, 2438
Höflich, P. 1995, ApJ, 443, 89
Höflich, P., & Khokhlov, A. 1996, ApJ, 457, 500
Höflich, P., Khokhlov, A., & Müller, E. 1992, A&A, 259, 549
———. 1993a, A&A, 268, 570
———. 1993b, A&AS, 97, 221
———. 1994, ApJS, 92, 501
Höflich, P., Khokhlov, A., Nomoto, K., Thielemann, F. K., & Wheeler, J. C. 1997, in Thermonuclear Supernovae, ed. P. Ruiz-Lapuente, R. Canal, & J. Isern (NATO ASI Ser. C, 486) (Dordrecht: Kluwer), 659
Höflich, P., Khokhlov, A., & Wheeler, J. C. 1995, ApJ, 444, 831
Hubbell, J. H. 1969, Photon Cross Sections, Attenuation Coefficients, and Energy Absorption Coefficients from 10 keV to 100 GeV (Natl. Stand. Ref. Data Ser. 29) (Washington: Natl. Bur. Stand.)
Iben, I., Jr., & Tutukov, A. V. 1984, ApJS, 54, 335
Johnson, W. N., et al. 1993, ApJS, 86, 693
Khokhlov, A. 1991, A&A, 245, 114
———. 1996, ApJ, 447, L73
Khokhlov, A., Müller, E., & Höflich, P. 1992, A&A, 253, L9
———. 1993, A&A, 270, 223
Khokhlov, A., Oran, E. S., & Wheeler, J. C. 1997a, ApJ, 478, 678
———. 1997b, Combustion Flame, 108, 503
Kirshner, R. P., et al. 1993, ApJ, 415, 589
Kumagai, K., & Nomoto, K. 1997, in Thermonuclear Supernovae, ed. P. Ruiz-Lapuente, R. Canal, & J. Isern (NATO ASI Ser. C, 486) (Dordrecht: Kluwer), 515
Leising, M. D., et al. 1995, ApJ, 450, 805
Lichti, G. G., et al. 1994, A&A, 292, 569
Livne, E., & Arnett, D. 1995, ApJ, 452, 62
Livne, E., & Glasner, A. S. 1990, ApJ, 361, 244
Matteson, M. 1997, in Workshop on Low/Medium Energy Gamma Ray Astrophysics Missions, Landsdown, Washington, November 1996
Meikle, W. P. S., et al. 1996, MNRAS, 281, 263
Niemeyer, J. C., & Hillebrandt, W. 1995, ApJ, 452, 769
Niemeyer, J. C., & Woosley, S. E. 1997, ApJ, 475, 740
Nomoto, K. 1981, in IAU Symp. 93, Fundamental Problems in the Theory of Stellar Evolution, ed. D. Sugimoto, D. Q. Lamb, & D. Schramm (Dordrecht: Reidel), 295
Nomoto, K. 1982, ApJ, 253, 798
Nomoto, K., & Sugimoto, D. 1977, PASJ, 29, 765
Nomoto, K., Thielemann, F.-K., & Yokoi, K. 1984, ApJ, 286, 644
Nugent, P., Baron, E., Branch, D., Fisher, A., & Hauschildt, P. H. 1997, ApJ, 485, 812
Perlmutter, S., et al. 1995, ApJ, 440, L41
Riess, A. G., Press, W. H., & Kirshner, R. P. 1996, ApJ, 473, 588
Ruiz-Lapuente, P., et al. 1993, Nature, 365, 728
Saha, A., Sandage, A., Labardt, L., Tammann, G. A., Macchetto, F. D., & Panagia, N. 1996, ApJS, 107, 693
Sandage, A., & Tammann, G. A. 1996, ApJ, 464, L51
Schmidt, B., et al. 1997, BAAS, in press
Thielemann, F.-K., Nomoto, K., & Hashimoto, M. 1994, in Supernovae, ed. S. Bludman, R. Mochkovitch, & J. Zinn-Justin (Amsterdam: Elsevier), 629
Veigele, W. J. 1973, At. Data Nucl. Data Tables, 5, 51
von Ballmoos, P., Dean, T., & Winkler, C. 1995, in Ann. NY Acad. Sci., 759, 17th Workshop on Relativistic Astrophysics, ed. H. Böhringer, G. E. Morfill, & J. E. Trümper, 401
Weaver, T. A., Axelrod, T. S., & Woosley, S. E. 1980, in Type I Supernovae, ed. J. C. Wheeler (Austin: Univ. Texas), 113
Webbink, R. F. 1984, ApJ, 277, 355
Wheeler, J. C. 1996, in Evolutionary Processes in Binary Stars, ed. R. A. M. Wijers, M. B. Davies, & C. A. Tout (NATO ASI Ser. C, 477) (Dordrecht: Kluwer), 307
Woosley, S. E., & Weaver, T. A. 1994, ApJ, 423, 371
Woosley, S. E., Weaver, T. A., & Taam, R. E. 1980, in Type I Supernovae, ed. J. C. Wheeler (Austin: Univ. Texas), 96